Quaternary Research 76 (2011) 452–459

Contents lists available at ScienceDirect

Quaternary Research

journal homepage: www.elsevier.com/locate/yqres

^{10}Be data from meltwater channels suggest that Jameson Land, east Greenland, was ice-covered during the last glacial maximum

Lena Håkansson [a,*], Jason P. Briner [b], Ala Aldahan [c,d], Göran Possnert [e]

[a] Geological Survey of Denmark and Greenland, Øster Voldgade 10, 1350 Copenhagen-K, Denmark
[b] Department of Geology, University at Buffalo, Buffalo, NY 14260, USA
[c] Department of Earth Sciences, Uppsala University, SE-752 36, Sweden
[d] Department of Geology, United Arab Emirates University, Al Ain, UAE
[e] Tandem Laboratory, Uppsala University, SE-751 21, Sweden

ARTICLE INFO

Article history:
Received 15 October 2010
Available online 9 August 2011

Keywords:
Greenland
Jameson Land
Glaciation
Last glacial maximum
Cosmogenic isotopes
Meltwater channels
Sandstone
Weathering

ABSTRACT

Along the northeast Greenland continental margin, bedrock on interfjord plateaus is highly weathered, whereas rock surfaces in fjord troughs are characterized by glacial scour. Based on the intense bedrock weathering and lack of glacial deposits from the last glaciation, interfjord plateaus have long been thought to be ice-free throughout the last glacial maximum (LGM). In recent years there is growing evidence from shelf and fjord settings that the northeast Greenland continental margin was more extensively glaciated during the LGM than previously thought. However, little is still known from interfjord settings. We present cosmogenic ^{10}Be data from meltwater channels and weathered sandstone outcrops on Jameson Land, an interfjord highland north of Scoresby Sund. The mean exposure age of samples from channel beds ($n = 3$) constrains on the onset of deglaciation on interior Jameson Land to 18.5 ± 1.3–21.4 ± 1.9 ka (for erosion conditions of 0–10 mm/ka, respectively). This finding adds to growing evidence that the northeast Greenland continental margin was more heavily glaciated during the LGM than previously thought.

Introduction

Identifying temporal and spatial changes of past ice sheets is critical for understanding their role in the global climate system. Within formerly glaciated regions, the occurrence of highly weathered terrain has often been used as evidence either for the existence of ice-free areas during the last glaciation (Ives, 1966; Nesje and Dahl, 1990; Ballantyne et al., 1998; Rae et al., 2004) or for the former distribution of cold-based ice allowing the preservation of pre-Pleistocene landscapes (Sugden, 1978; Kleman, 1994; Sollid and Sørbel, 1994; Kleman and Hätterstrand, 1999). In recent years, cosmogenic exposure dating methods have provided a new technique to interpret differentially weathered landscapes, which has led to a new understanding of the extent and dynamics of ice sheets (Bierman et al., 1999; Marsella et al., 2000; Fabel et al., 2002; Stroeven et al., 2002; Briner et al., 2003, 2005, 2006; Landvik et al., 2003; Marquette et al., 2004; Davis et al., 2006; Phillips et al., 2006; Darmody et al., 2008).

Along the northeast Greenland continental margin (Fig. 1), from Scoresby Sund and northwards, bedrock on interfjord plateaus is highly weathered whereas rock surfaces in fjord troughs are characterized by glacial scour. Previous work suggested that the different degree of weathering from plateau to fjord exists because interfjord plateaus remained ice-free throughout the last glacial cycle whereas fjords where occupied by outlet glaciers from the ice sheet (Funder and Hjort, 1973; Hjort, 1979, 1981; Dowdeswell et al., 1994; Funder and Hansen, 1996; Funder et al., 1994, 1998). Based on the intense bedrock weathering and lack of glacial deposits from the last glaciation on interior Jameson Land, the area has long been thought to be ice-free throughout the last glacial maximum (LGM) (Funder and Hjort, 1973; Funder, 1989; Möller et al., 1994; Funder and Hansen, 1996; Funder et al., 1994, 1998).

Jameson Land, east Greenland

The Jameson Land peninsula (70°–71°N) is located at the northern side of Scoresby Sund, the largest fjord system in east Greenland (Fig. 1). The distance between the fjord mouth and the present margin of the Greenland Ice Sheet is ~200 km. The Scoresby Sund region is dominated by three landscape types (Fig. 1): (i) closest to the ice-sheet margin, deep fjords are cut into ice-covered high mountain plateaus of crystalline bedrock, (ii) north of Scoresby Sund, on the Jameson Land peninsula, Mesozoic sandstone and shale make up low-relief, ice-free terrain, and (iii) south of Scoresby Sund and east of Jameson Land the landscape is alpine with high relief.

Håkansson et al. (2007) presented ^{10}Be ages from erratics on Kap Brewster, at the mouth of Scoresby Sund at 250 m asl (Fig. 1). The

* Corresponding author.
E-mail address: leh@geus.dk (L. Håkansson).

0033-5894/$ – see front matter © 2011 University of Washington. Published by Elsevier Inc. All rights reserved.
doi:10.1016/j.yqres.2011.06.007

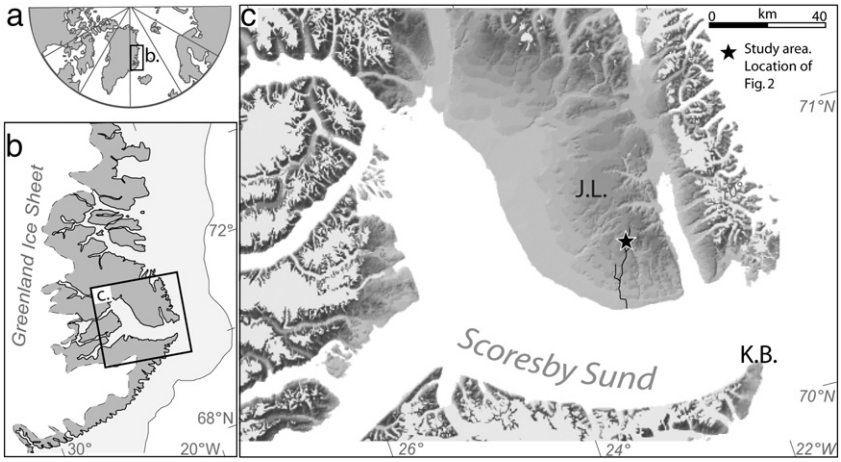

Figure 1. Maps showing: (a) the Arctic and the location of Greenland, and (b) northeast Greenland, with the continental shelf marked with light gray. (c) The Scoresby Sund area: J.L. = Jameson Land; K.B. = Kap Brewster. The Fynselv River and the study area are marked on the map.

finding suggests that active ice at the mouth of Scoresby Sund reached at least 250 m asl during the LGM, and imply a more extensive Greenland Ice Sheet cover over Jameson Land during the LGM than previously thought. In addition, ^{10}Be and ^{26}Al measurements from far-traveled erratic boulders on Jameson Land indicate deposition by an extensive advance of the Greenland Ice Sheet over Jameson Land during Marine Isotope Stage (MIS) 6 and prior to MIS 6 (Håkansson et al., 2009). This is consistent with previous studies based on stratigraphy in the region (Möller et al., 1994; Funder et al., 1998; Adrielsson and Alexanderson, 2005). A subset of younger ^{10}Be ages suggests that local cold-based ice caps covered interior Jameson Land for some portion of the last glacial cycle (Håkansson et al., 2009). It is, however, inconclusive whether or not the area was covered by ice during the LGM.

In the present study, we test if Jameson Land indeed was covered by a local ice cap during the LGM; we use cosmogenic ^{10}Be data from meltwater channels and weathered sandstone outcrops to constrain the timing of meltwater incision, which in turn can estimate the timing of the onset of deglaciation on interior Jameson Land.

Geomorphology of the study area

Description

The Jameson Land Peninsula has an asymmetric topographic profile. From the plateau areas of interior Jameson Land the terrain gently slopes towards Scoresby Sund in the west and south whereas the eastern margin, facing Hurry Fjord, has a steeper gradient (Fig. 1). The plateaus form the watershed between east-draining rivers towards Hurry Fjord and the many (and commonly large) river valleys draining west and south towards Scoresby Sund. South of the plateaus there are extensive areas with exposed weathered Jurassic sandstone, most of which are concentrated along the middle Fynselv River and its tributaries (Fig. 1c; Schunke, 1986; Hjort and Salvigsen, 1991; Möller et al., 1994; Ronnert and Nyborg, 1994). We here focus on an interfluve plateau bounded by the deep canyons of the Fynselv River to the east and by one of the Fynselv tributaries to the west (Figs. 2, 3a).

In the study area, the distribution of weathered sandstone outcrops, meltwater channels and patches of ground moraine was mapped using 1:50,000-scale aerial photographs. The map was ground-truthed and further modified in the field (Fig. 2). The studied interfluve plateau is 3 km wide and 5 km long, and located at 350–550 m asl (~70°38′N, 23°07′W). It is bounded by >100-m-deep v-shaped canyons (Figs. 2, 3a). The interior of the interfluve is covered by regolith, which comprises granular grus (<0.5 m deep) and larger blocks including cobbles and boulders (Fig. 3b). Weathered sandstone outcrops are concentrated along the edges of the interfluve and are incised by channels (Fig. 2). Two channel types are represented (Fig. 2): (i) dendritic channel systems with a series of feeder tributaries (1–20 m wide, <10 m deep, Fig. 2c) that drain into one larger channel, and (ii) wide channels (>30 m across, <6 m deep, Fig. 3d) that start abruptly and terminate above cliffs along major canyons ('hanging valleys'; Hjort and Salvigsen, 1991). Both channel types are controlled by the rhombic pattern of fractures in the sandstone and their gradients follow the topography. Thin patches of ground moraine occur in the area (Fig. 2) and are further described and dated in Håkansson et al. (2009).

There is a transition in the degree of weathering from channel beds to the surrounding sandstone outcrops. Based on the degree of weathering we classify the sandstone surfaces in three groups: (i) channel beds, (ii) surfaces adjacent to channel beds, and (iii) weathered surfaces. The sandstone-floored channel beds are the freshest surfaces; they are smooth and rarely show weathered relief >5 cm. In contrast, highly weathered surfaces are situated away from the channels and show rounded weathering features (Fig. 3e), pedestals (Fig. 3f) and circular weathering pits up to 20 cm deep. Weathered surfaces (Fig. 3g) are found either on undulating outcrops or on tors rising conspicuously above the surroundings; honeycomb weathering is only found on well-developed tors (Fig. 3h). Surfaces adjacent to channels are a transition zone between fresh channel beds and the surrounding highly weathered bedrock. These surfaces are undulating and have a surface texture much like the channel beds; however, occasional weathering pits measure ca. 10 cm deep.

Interpretation

The incision of channels on the interfluve surface requires a significant amount of flowing water more than 100 m above the modern-day drainage, which is the depth of the surrounding canyons. Thus, the observed channel systems are difficult to explain by modern fluvial erosion; we interpret them as having been eroded by glacier-derived meltwater. All channels follow the topographic gradient indicating that drainage was controlled by the topography rather than by pressure head in a subglacial setting. Channels are interpreted as having formed in front of or along the ice margin. The transition in the degree of weathering from fresh channel beds to the surrounding weathered sandstone outcrops indicates that: (i) channel beds and surfaces adjacent to channels have been eroded during the last deglaciation of the area when ice was stagnant and crevassed, and (ii) the delicate features of weathered surfaces have been preserved

https://doi.org/10.1016/j.yqres.2011.06.007 Published online by Cambridge University Press

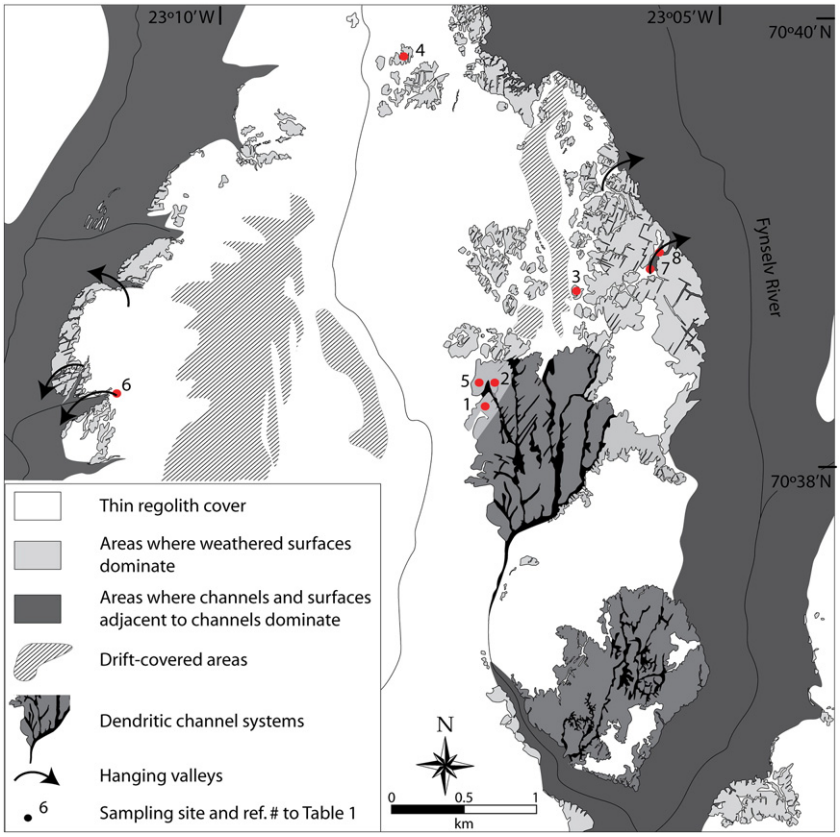

Figure 2. Map of the studied interfluve plateau study area illustrating the distribution of channels and areas where weathered surfaces and surfaces adjacent to channels dominate. Sample positions are shown with reference numbers to Table 1. The map is based on aerial photographs and field mapping.

beneath non-erosive ice. Hence, the morphology suggests that channel beds are younger relative to the weathered sandstone surfaces.

Cosmogenic ^{10}Be

Methods

Samples for measurement of cosmogenic ^{10}Be concentration were collected from sandstone surfaces using hammer and chisel. The position and elevation of samples were obtained using a hand-held GPS receiver (uncertainty ±10 m), and shielding from the surrounding horizon was measured with a compass and clinometer. Samples were processed for ^{10}Be analysis at the University at Buffalo following procedures modified after Kohl and Nishiizumi (1992) and Briner (2003). About 40 g of clean quartz from each sample was dissolved in batches of 11 and one process blank (Table 1). Known amounts of SPEX-brand Be carrier (1000 ml/l) were added to all samples and to the process blank. ^{10}Be/^{9}Be ratios were measured at the Tandem Laboratory at Uppsala University and at PRIME lab, Purdue University. The CRONUS-Earth exposure age calculator version 2.2 has been used to calculate model ages (Balco et al., 2008; http://hess.ess.washington.edu/math/). This version of the calculator uses the revised ^{10}Be decay constant of $5.10 \pm 0.26 \times 10^{-7}$ yr^{-1} (Nishiizumi et al., 2007). Ages were calculated with a regionally calibrated ^{10}Be production rate for northeastern North America (Balco et al., 2009), the scaling scheme by Lal (1991) and Stone (2000) and a constant production rate model (2σ, sea level, high latitude and standard atmosphere). Correction was made for altitude, shielding by the surrounding horizon and for sample thickness using exponential decrease in nuclide production and a bulk density for sandstone of 2.38 g cm^{-1}.

Results

Fourteen ^{10}Be measurements show that the isotope concentrations (and model ages) are closely correlated with the degree of bedrock weathering. The weathered surfaces have the highest concentrations and meltwater channels have the lowest (Table 1; Fig. 4). All model ages are calculated assuming no subaerial postglacial erosion (Table 1). Four samples from weathered sandstone surfaces have minimum ^{10}Be ages ranging from 33.0 ± 2.1 to 58.3 ± 3.6 ka, with a mean age of 43.6 ± 2.8 ka. Seven ^{10}Be ages from surfaces adjacent to channels range from 20.7 ± 2.0 to 40.0 ± 2.6 ka, and give a mean age of 28.9 ± 2.4 ka. Three samples from channel beds of 'hanging valleys' yield ^{10}Be ages ranging from 16.9 ± 1.1 to 20.3 ± 1.5 ka, with a mean age of 18.5 ± 1.3 ka. The model ages from the three surface types have been analyzed with one-way analyses of variance (ANOVA) to test for the statistical separability of the populations. Model ages of the three groups differ significantly, $F(2, 11) = 9.5$ $p < 0.004$.

Discussion

^{10}Be ages

Recent research shows that regional production rates in northeastern North America (Balco et al., 2009), Norway (Goehring et al., in press) and New Zealand (Putnam et al., 2010) are ca. 6–14% lower than production rates based on the commonly accepted global ^{10}Be calibration dataset (Balco et al., 2009). We choose to calculate ^{10}Be ages with the regionally

https://doi.org/10.1016/j.yqres.2011.06.007 Published online by Cambridge University Press

Figure 3. Photos describing the investigated interfluve plateau. (a) The deep canyon of the Fynselv River. (b) Regolith cover on the interior of the investigated plateau. (c) A narrow tributary channel in one of the dendritic channel systems. (d) Wide channel ('hanging valley') ca. 30 m across. (e) Rounded weathering features. (f) Pedestals (g) weathered surface, position of sample 06-FE-56. (h) Tor with honeycomb weathering.

calibrated North American ^{10}Be production rate (Balco et al., 2009), which has recently been applied in western Greenland (Young et al., 2011).

Here, model ages are presented with no subaerial erosion because there is no local erosion rate information, and the use of an erosion correction for all samples would presume continuous exposure and steady erosion, neither of which is thought to be the case for the weathered surfaces or surfaces adjacent to channel beds. Therefore, all model ages are presented as minimum limiting ages. However, the weathered relief of channels and surfaces adjacent to channels indicates that there indeed has been subaerial postglacial erosion. Sandstone weathering rates of >5 mm ka^{-1} have been estimated from arctic settings (Linge et al., 2006). We have applied postglacial weathering rates of 5 and 10 mm ka^{-1} to test for the effect of reasonable erosion rates, which would increase the mean age of channel beds from 18.5 ± 1.3 ka to 19.8 ± 1.6 and 21.4 ± 1.9 ka, respectively.

Interpreting ^{10}Be concentrations from arctic landscapes is challenging, especially where cold-based ice has been present (Davis et al., 1999; Briner et al., 2006; Håkansson et al., 2009). The calculation of cosmogenic exposure ages relies on the assumptions that a sampled surface has been constantly exposed and lacks inherited isotopes from previous exposures, requiring at least ca. 2 m of glacial erosion and furthermore, experienced only minimal post-glacial surface erosion. This is the case for most heavily scoured bedrock surfaces in settings where substantial glacial erosion took place (e.g., within fjords). However, for weathered bedrock surfaces in areas covered by non-erosive ice, the concentration of isotopes comprises not only isotopes produced since the last deglaciation, but also inherited isotopes from previous exposure (Davis et al., 1999; Briner et al., 2006). The morphology of the study area on Jameson Land suggests that weathered surfaces were preserved beneath non-erosive ice and that channels were incised upon deglaciation. Thus, we interpret the relatively high isotope concentrations in weathered surfaces as a result of inheritance and the mean exposure age of samples from channel beds

https://doi.org/10.1016/j.yqres.2011.06.007 Published online by Cambridge University Press

Table 1
Sample details and ^{10}Be model ages.

Sample	Original AMS lab nr	Site no. in Figure 2	AMS facility	Latitude (°N)	Longitude (°W)	Elevation (m asl)	Carrier[c] weight (mg)	Quartz weight (g)	Sample thickness (cm)	Shielding correction	^{10}Be/^{9}Be not blank corrected (10^{-13})	^{10}Be/^{9}Be [d] Blank (10^{-14})	% of ratio represented by the blank error (2σ)	^{10}Be [e] (10^{5} atoms g^{-1})	^{10}Be age [f,g] (ka) error (2σ)
Weathered surfaces															
06-FE-5	06-FE-5	1	Uppsala [a]	70°38.08′	23°08.18′	495	0.3493	40.01	2	1	5.54 ± 0.29	1.79 ± 0.36	3.22%	3.13 ± 0.15	42.2 ± 2.9
06-FE-56	79,963	2	PRIME [b]	70°38.31′	23°07.75′	462	0.3582	40.83	2	1	7.26 ± 0.27	3.74 ± 0.86	5.15%	4.29 ± 0.16	58.3 ± 3.6
06-FE-65	70,061	3	PRIME	70°38.70′	23°06.55′	456	0.3503	41.31	2	1	5.24 ± 0.21	3.74 ± 0.86	7.13%	2.97 ± 0.12	40.8 ± 2.6
06-FE-67	79,965	4	PRIME	70°39.97′	23°07.12′	490	0.3569	40.11	2	1	4.19 ± 0.18	3.74 ± 0.86	8.92%	2.49 ± 0.25	33.0 ± 2.1
Surfaces adjacent to channels															
06-FE-55	79,962	2	PRIME	70°38.05′	23°07.89′	443	0.3581	39.96	2	1	4.39 ± 0.31	3.74 ± 0.86	8.52%	2.63 ± 0.18	36.4 ± 3.1
06-FE-48	06-FE-48	5	Uppsala	70°38.32′	23°08.13′	470	0.3575	39.20	2	1	3.37 ± 0.33	3 ± 0.82	8.90%	1.87 ± 0.15	25.7 ± 2.5
06-FE-46	06-FE-46	5	Uppsala	70°38.35′	23°08.08′	524	0.3513	40.94	2	1	5.51 ± 0.3	1.79 ± 0.36	3.24%	3.06 ± 0.31	40.0 ± 2.8
06-FE-50	06-FE-50	5	Uppsala	70°38.32′	23°08.13′	470	0.3532	40.01	2	1	4.04 ± 0.23	1.79 ± 0.36	4.43%	2.28 ± 0.23	31.3 ± 2.2
06-FE-57	06-FE-57	2	Uppsala	70°38.19′	23°07.96′	449	0.3541	40.16	2	1	3.11 ± 0.2	1.79 ± 0.36	5.74%	1.73 ± 0.17	24.2 ± 1.8
06-FE-53	06-FE-53	2	Uppsala	70°38.00′	23°08.04′	430	0.2709	40.67	2	1	3.92 ± 0.25	1.79 ± 0.36	4.56%	1.67 ± 0.17	23.8 ± 1.8
06-FE-51	06-FE-51	2	Uppsala	70°38.15′	23°08.05′	444	0.3572	40.14	2	1	2.77 ± 0.29	3 ± 0.82	10.83%	1.47 ± 0.15	20.7 ± 2.2
Channel beds															
06-FE-19	06-FE-19	6	Uppsala	70°38.40′	23°12.70′	377	0.3587	40.01	2	1	2.29 ± 0.14	4.15 ± 0.48	18.10%	1.13 ± 0.11	16.9 ± 1.1
06-FE-25	06-FE-25	7	Uppsala	70°38.59′	23°05.87′	500	0.354	40.89	2	0.989	2.52 ± 0.18	1.79 ± 0.36	7.09%	1.36 ± 0.14	18.3 ± 1.4
06-FE-24	79,966	8	PRIME	70°39.15′	23°05.90′	510	0.349	40.01	2	0.968	2.6 ± 0.14	3.74 ± 0.86	14.36%	1.52 ± 0.15	20.3 ± 1.5

[a] Tandem Laboratory, Uppsala University, NIST SRM4325 Be-standardization with assumed isotope ratio of $3.03 * 10^{-11}$.
[b] PRIME lab, Purdue Univesity, KNSTD Be-standardization $2.79 * 10^{-11}$.
[c] Weight of Spex 1000 Be carrier (^{9}Be concentration:1000 ml/l).
[d] Samples are dissolved in different batches and have thus been corrected for the specific blank of each batch.
[e] Isotopic concentrations are not corrected for elevation, latitude and shielding.
[f] Model ages are calculated with no erosion and standard pressure.
[g] Reference ^{10}Be production rate due to spallation 3.93 ± 0.19 atoms g^{-1} yr^{-1}, based on the northeastern North American calibration data set (Balco et al., 2009) and the standard scaling scheme of Lal (1991) and Stone (2000).

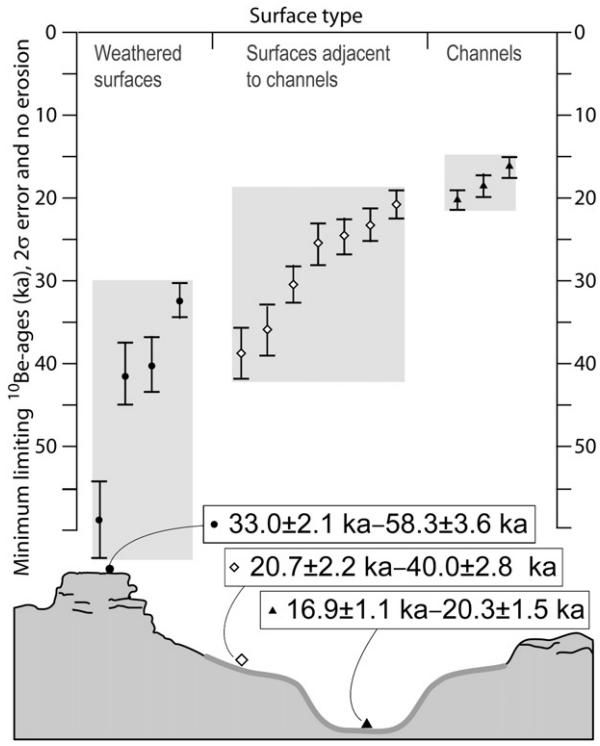

Figure 4. (a) Distribution of ^{10}Be-model ages (within 2-sigma error and assuming no erosion; see Table 1). (b) Profile showing a conceptual transect from meltwater channel bed to weathered surfaces. The range of ^{10}Be-model ages for each surface type is shown.

(18.5 ± 1.3 ka) as constraining the timing of the last glaciation on interior Jameson Land.

There is, however, an alternative interpretation that might yield young channel ages relative to ages from adjacent, weathered surfaces. It is possible that the last glaciation of interior Jameson Land occurred earlier, prior to the LGM, and the channel beds have relatively young exposure ages because they were occupied and shielded by snow or ice until ca. 18.5 ka. To completely shield a surface from cosmic radiation would require tens of meters of snow shielding, or ~10 m of shielding by ice (Miller et al., 2006). Our study area has low relief and the sampled meltwater channels are <6 m deep; thus, it is unlikely that only the channel beds have been shielded.

Two scenarios are possible to completely shield the channel beds: (i) stagnant ice lingered in the area following channel incision, or (ii) >10 m of snow accumulated over the area right after deglaciation. Neither of these scenarios are likely: (i) the channel systems are interpreted as having been formed in a subaerial environment in front of and along the ice margin and therefore it is unlikely that thick ice remained over the area by the time that channels were incised. And, (ii) the nearby Renland ice core indicates that accumulation throughout the last glacial cycle was only ca. 20–30% of the present accumulation. The annual precipitation of the region is low (151 mm/yr at Scoresbysund weather station; Yang et al., 1999) and therefore it is unlikely that tens of meters of snow accumulated fast enough to inhibit ^{10}Be production of >>18.5 ka. We suggest that the most likely explanation is that channels were eroded by meltwater during deglaciation by a local ice cap following the LGM.

Glacial history of the Scoresby Sund region

The culmination of the last glaciation that reached the continental shelf off Scoresby Sund is constrained by marine cores documenting an increased sediment flux to the shelf slope between 21 and 16 cal ka BP (Nam et al., 1995; Stein et al., 1996). A distinct shift in oxygen isotope ratios at ca. 15 cal ka BP is suggested to mark a meltwater pulse linked with ice retreat (Nam et al., 1995). The timing of deglaciation from the fjord mouth is constrained by ^{10}Be ages from erratics (Håkansson et al., 2007). The ^{10}Be ages were re-calculated in this study using the northeastern North American calibration dataset by Balco et al. (2009) and indicate deglaciation from the fjord mouth already between 16.6 ± 2.5 and 18.9 ± 3.3 ka (calculated with 0–10 mm/ka erosion conditions, respectively). Our average ^{10}Be ages of channel beds (18.5 ± 1.3–21.4 ± 1.9 ka, with 0–10 mm/ka erosion) overlap within 2-sigma error with the ^{10}Be ages from the fjord mouth (Håkansson et al., 2007) and indicate early deglaciation both on interior Jameson Land and from the outer fjord. Such early deglaciation has also been suggested for the southern sector of the Greenland Ice Sheet where deglaciation commenced before 19 ka (Carlson et al., 2008).

There are, however, two potential scenarios that would alter channel ages either making them younger or even older. First, insufficient meltwater erosion during deglaciation (<2 m) would result in inherited isotopes and channel bed ages that are slightly too old. Alternatively, if channel beds experienced even more postglacial erosion than predicted and/or seasonal snow cover, then this would result in even older channel ages.

In any case, based on the ^{10}Be dated erratics perched on 250 m asl at the fjord mouth, Håkansson et al. (2007) proposed that active ice in the fjord trough during the LGM must have been buttressed by cold-based ice over the weathered interior of the Jameson Land peninsula. Therefore we suggest that our ^{10}Be ages from channel beds indeed indicate that Jameson Land was covered by a non-erosive local ice cap during the LGM.

Conclusion

In this study we present cosmogenic ^{10}Be data from weathered sandstone outcrops and meltwater channel beds on the Jameson Land peninsula, east Greenland. The presence of meltwater channels requires

https://doi.org/10.1016/j.yqres.2011.06.007 Published online by Cambridge University Press

that the study area was covered by glacial ice. The morphology of weathered surfaces suggests that this ice must have been minimally erosive to allow for preservation of delicate weathering features. The mean exposure age of samples from channel beds constrains on the onset of deglaciation on interior Jameson Land between 18.5 ± 1.3 and 21.4 ± 1.9 ka (for erosion conditions of 0–10 mm/ka, respectively). This finding adds to growing evidence that the northeast Greenland continental margin was more heavily glaciated during the LGM than previously thought.

Acknowledgments

This research was funded by the Helge Ax:son Johnson Foundation and Fysiografiska Sällskapet, Lund. The Danish Polar Centre and POLOG provided logistic support. Elizabeth Thomas is acknowledged for enthusiastic help and great company in the field. Nicolaj Krog Larsen, Lena Adrielsson and Christian Hjort are thanked for valuable discussions on this manuscript. Paul Bierman and an anonymous reviewer are thanked for constructive criticism that has significantly improved this manuscript.

References

Adrielsson, L., Alexanderson, H., 2005. Interactions between the Greenland Ice Sheet and the Liverpool Land coastal ice cap during the last two glaciation cycles. Journal of Quaternary Science 20 (3), 269–283.

Ballantyne, C.K., McCarroll, D., Nesje, A., Dahl, S.O., 1998. The last ice sheet in North-West Scotland: reconstruction and implications. Quaternary Science Reviews 17, 1149–1184.

Balco, G., Stone, J.O., Lifton, N.A., Dunai, T.J., 2008. A complete and easily accessible means of calculating surface exposure ages or erosion rates from ^{10}Be and ^{26}Al measurements. Quaternary Geochronology 3, 174–195.

Balco, G., Briner, J., Finkel, R.C., Rayburn, J.A., Ridge, J.C., Schaefer, J.M., 2009. Regional beryllium-10 production rate calibration for northeastern North America. Quaternary Geochronology 4, 93–107.

Bierman, P.R., Marsella, K.A., Patterson, C., Davis, P.T., Caffee, M., 1999. Mid-Pleistocene cosmogenic minimum-age limits for pre-Wisconsinan glacial surfaces in southwestern Minnesota and southern Baffin Island; a multiple nuclide approach. Geomorphology 27, 25–39.

Briner, J.P., 2003. The last glaciation of the Clyde region, north-eastern Baffin Island, arctic Canada: cosmogenic isotopes constraints on Laurentide Ice Sheet dynamics and chronology. Ph.D. dissertation, University of Colorado, Boulder, pp. 300.

Briner, J.P., Miller, G., Davies, P.T., Bierman, P.R., Caffee, M., 2003. Last glacial maximum ice sheet dynamics in the Canadian Arctic inferred from young erratics perched on ancient tors. Quaternary Science Reviews 22, 437–444.

Briner, J.P., Miller, G.H., Davis, T., Finkel, R., 2005. Cosmogenic exposure dating in arctic glacial landscapes: implications for the glacial history of north-eastern Baffin Island, Arctic Canada. Canadian Journal of Earth Sciences 42, 67–84.

Briner, J.P., Miller, G., Davies, P.T., Finkel, R., 2006. Cosmogenic radionuclides from fiord landscapes support differential erosion by overriding ice sheets. GSA Bulletin 118, 406–430.

Carlson, A., Stoner, J.S., Donnelly, J.P., Hillaire-Marcel, C., 2008. Response of the southern Greenland Ice Sheet during the last two deglaciations. Geology 36, 359–362.

Darmody, R.G., Thorn, C.E., Seppälä, M., Campbell, S.W., Li, Y.K., Harbour, J., 2008. Age and weathering status of granite tors in Arctic Finland (68 N°). Geomorphology 94, 10–23.

Davis, P.T., Bierman, P.R., Marsella, K.A., Caffee, M.W., Southon, J.R., 1999. Cosmogenic analysis of glacial terrains in the eastern Canadian Arctic: a test for inherited nuclides and the effectiveness of glacial erosion. Annals of Glaciology 28, 181–188.

Davis, P.T., Briner, J.P., Coulthard, R.P., Finkel, R.W., Miller, G.H., 2006. Preservation of Arctic landscapes overridden by cold-based ice sheets. Quaternary Research 65, 156–163.

Dowdeswell, J.A., Uenzelmann-Neben, G., Whittington, R.J., Marienfeld, P., 1994. The Late Quaternary sedimentary record in Scoresby Sund, East Greenland. Boreas 23, 294–310.

Fabel, D., Stroeven, A.P., Harbour, J., Kleman, J., Elmore, D., Fink, D., 2002. Landscape preservation under Fennoscandian ice sheets determined from in situ produced ^{10}Be and ^{26}Al. Earth and Planetary Science Letters 201, 397–406.

Funder, S., 1989. Quaternary geology of the ice-free areas and adjacent shelfs of Greenland; Chapter 13. In: Fulton, R.J. (Ed.), Quaternary Geology of Canada and Greenland, Geological Survey of Canada, pp. 742–792.

Funder, S., Hansen, L., 1996. The Greenland Ice Sheet — a model for its culmination and decay during and after the last glacial maximum. Bulletin of the Geological Society of Denmark 42, 137–152.

Funder, S., Hjort, C., 1973. Aspects of the Weichselian chronology in central East Greenland. Boreas 2, 69–84.

Funder, S., Hjort, C., Landvik, J.Y., 1994. The last glacial cycle in East Greenland, an overview. Boreas 23, 283–293.

Funder, S., Hjort, C., Landvik, J.Y., Nam, S.-I., Reeh, N., Stein, R., 1998. History of a stable ice margin — East Greenland during the middle and upper Pleistocene. Quaternary Science Reviews 17, 77–123.

Goehring, B.M., Lohne, Ø., Mangerud, J., Svendsen, J.I., Gyllencreutz, R., Schaefer, J., Finkel, R., in press. Late Glacial and Holocene Beryllium-10 production rates for western Norway.

Hjort, C., 1979. Glaciation in northern East Greenland during the Late Weichselian and Early Flandrian. Boreas 8, 281–296.

Hjort, C., 1981. A glacial chronology for northern East Greenland. Boreas 10, 259–274.

Hjort, C., Salvigsen, O., 1991. The channel and tor landscape in southeastern Jameson Land, East Greenland. LUNDQUA Report 33, 23–26.

Håkansson, L., Briner, J.P., Alexanderson, H., Aldahan, A., Possnert, G., 2007. ^{10}Be ages from coastal northeast Greenland constrain the extent of the Greenland Ice Sheet during the last glacial maximum. Quaternary Science Reviews 26, 2316–2321.

Håkansson, L., Alexanderson, H., Hjort, C., Möller, P., Briner, J.P., Aldahan, A., Possnert, G., 2009. The late Pleistocene glacial history of Jameson Land, central East Greenland derived from cosmogenic ^{10}Be and ^{26}Al exposure dating. Boreas 38 (2), 244–260.

Ives, J.D., 1966. Blockfields, associated weathering forms on mountain tops and the nunatak hypothesis. Geografiska Annaler 48A, 220–223.

Kleman, J., 1994. Preservation of landforms under ice sheets and ice caps. Geomorphology 9, 19–32.

Kleman, J., Hätterstrand, C., 1999. Frozen-bed Fennoscandian and Laurentide ice sheets during the Late Glacial Maximum. Nature 402, 63–66.

Kohl, C.P., Nishiizumi, K., 1992. Chemical isolation of quartz for measurement of in-situ produced cosmogenic nuclides. Geochimica et Cosmochimica Acta 56, 3583–3587.

Lal, D., 1991. Cosmic ray labeling of erosion surfaces: in-situ nuclide production rates and erosion models. Earth and Planetary Science Letters 104, 424–439.

Landvik, J.Y., Brook, E.J., Gualtieri, L., Raisbeck, G., Salvigsen, O., Yiou, F., 2003. Nortwest Svalbard during the last glaciation: ice-free areas existed. Geology 31, 905–908.

Linge, H., Larsen, E., Kjaer, K.H., Demidov, I.N., Brook, E.J., Raisbeck, G.M., Yiou, F., 2006. Cosmogenic ^{10}Be exposure age dating across Early to Late Weichselian ice-marginal zones in northwestern Russia. Boreas 35, 576–586.

Marsella, K.A., Bierman, P.R., Davis, P.T., Caffee, M.W., 2000. Cosmogenic ^{10}Be and ^{26}Al ages for the last glacial maximum, eastern Baffin Island, Arctic Canada. Geological Society of America Bulletin 112, 1296–1312.

Marquette, G.C., Gray, J.T., Gosse, J.C., Courchesne, F., Stockli, L., Macpherson, G., Finkel, R., 2004. Felsenmeer persistence under non-erosive ice in the Torngat Mountains and Kaumajet Mountains, Quebec and Labrador, as determined by soil weathering and cosmogenic nuclide exposure dating. Canadian Journal of Earth Sciences 41, 19–38.

Miller, G.H., Briner, J.P., Lifton, N.A., Finkel, R.C., 2006. Limited ice-sheet erosion and complex exposure histories derived from in situ cosmogenic ^{10}Be, ^{26}Al and 14°C on Baffin Island, Arctic Canada. Quaternary Geochronology 1, 74–85.

Möller, P., Hjort, C., Adrielsson, L., Salvigsen, O., 1994. Glacial history of interior Jameson Land, East Greenland. Boreas 23, 320–348.

Nam, S.-I., Stein, R., Grobe, H., Hubberten, H., 1995. Late Quaternary glacial/interglacial changes in sediment composition at the East Greenland continental margin and their paleoceanographic implications. Marine Geology 122, 243–262.

Nesje, A., Dahl, S.O., 1990. Autochthonous block fields in southern Norway — implications for the geometry, thickness an isostatic loading of the Late Weichselian Scandinavian Ice Sheet. Journal of Quaternary Science 5, 225–234.

Nishiizumi, K., Imamura, M., Caffee, M.W., Southon, J.R., Finkel, R.C., McAninch, J., 2007. Absolute calibration of ^{10}Be AMS standards. Nuclear Instruments and Methods in Physics Research B 258, 403–413.

Phillips, W.M., Hall, A.M., Mottram, R., Fifield, L.K., Sugden, D.E., 2006. Cosmogenic ^{10}Be and ^{26}Al exposure ages of tors and erratics, Cairngorm Mountains, Scotland: timescales for the development of a classic landscape of selective linear glacial erosion. Geomorphology 73, 222–245.

Putnam, A., Schaefer, J.M., Vandergoes, M., Barrell, D., Denton, G.H., Kaplan, M., Schwartz, R., Finkel, R.C., Goehring, B.M., Kelley, S.E., 2010. In situ cosmogenic ^{10}Be production rate from the Southern Alps, New Zealand. Quaternary Geochronology 5, 392–409.

Rae, A.C., Harrison, S., Mighall, T., Dawson, A.G., 2004. Periglacial trimlines and nunataks of the last glacial maximum: the Gap of Dunloe, southwest Ireland. Journal of Quaternary Science 19, 87–97.

Ronnert, L., Nyborg, M.R., 1994. The distribution of different glacial landscapeson southern Jameson Land, East Greenland according to Landsat Thematic Mapper data. Boreas 23, 294–311.

Schunke, E., 1986. Periglazialformen und Morphodynamik im südlichen Jameson Land, Ost-Grönland. Abhandlungen der Akademie der Wissenschaften in Göttingen. 142 pp.

Sollid, J.L., Sørbel, L., 1994. Distribution of glacial landforms I Southern Norway in relation to the thermal regime of the Last Continental Ice Sheet. Geografiska Annaler 76, 25–36.

Stein, R., Nam, S.-I., Grobe, H., Huberten, H., 1996. Late Quaternary glacial history and short-term ice rafted debris fluctuations along the east Greenland continental margin. In: Andrews, et al. (Ed.), Late Quaternary

Paleoceanography of the North Atlantic Margins: Geological Society Special Publication, 111, pp. 135–151.
Stone, J.O., 2000. Air pressure and cosmogenic isotope production. Journal of Geophysical Research 105, 23753–23759.
Stroeven, A.P., Fabel, D., Hättestrand, C., Harbour, J., 2002. A relict landscape in the centre of the Fennoscandian glaciation: cosmogenic radionuclide evidence of tors preserved through multiple glacial cycles. Geomorphology 44, 145–154.
Sugden, D.E., 1978. Glacial erosion by the Laurentide Ice Sheet. Journal of Glaciology 83, 367–391.
Yang, D.Q., Ishida, S., Goodison, B.E., Gunther, T., 1999. Bias correction of daily precipitation measurements for Greenland. Journal of Geophysical Research — Athmospheres 104, 6171–6181.
Young, N.E., Briner, J.P., Stewart, H.A.M., Axford, Y., Csatho, B., Rood, D.H., Finkel, R.C., 2011. Response of Jakobshavn Isbræ, Greenland, to Holocene climate change. Geology 39, 131–134.

https://doi.org/10.1016/j.yqres.2011.06.007 Published online by Cambridge University Press